ELSEVIER

Contents lists available at ScienceDirect

# Computers and Electronics in Agriculture

journal homepage: www.elsevier.com/locate/compag



# Original papers



# Automated in-field leaf-level hyperspectral imaging of corn plants using a Cartesian robotic platform

Ziling Chen<sup>a</sup>, Jialei Wang<sup>b</sup>, Tao Wang<sup>c</sup>, Zhihang Song<sup>a</sup>, Yikai Li<sup>a</sup>, Yuanmeng Huang<sup>a</sup>, Liangju Wang<sup>a</sup>, Jian Jin<sup>a,\*</sup>

- <sup>a</sup> Department of Agricultural and Biological Engineering, Purdue University, West Lafayette, IN 47907, United States
- <sup>b</sup> School of Mechanical Engineering, Purdue University, West Lafayette, IN 47907, United States
- <sup>c</sup> College of Biosystems Engineering and Food Science, Zhejiang University, Zhejiang 310058, China

#### ARTICLE INFO

# ABSTRACT

Keywords: Crop leaf scanner Plant phenotyping Hyperspectral imaging Cartesian robot Robotic system Hyperspectral Imaging (HSI) has been widely adopted in field plant phenotyping activities. Current HSI solutions such as airborne remote sensing platforms and handheld spectrometers have been proven effective and have become popular in various phenotyping applications. However, the imaging quality of current airborne sensing systems still suffers from various noises due to the changing ambient lighting condition, long imaging distance, and comparatively low resolution. Handheld leaf spectrometers provide a higher quality of spectral data, but they only measure a small spot on the leaf, which cannot represent the whole leaf or canopy very well due to the great variation between different locations. In 2018, the Purdue Ag engineers developed a new handheld hyperspectral leaf imager, LeafSpec. For the first time, phenotyping researchers were able to collect highresolution hyperspectral leaf images without the impacts of the changing ambient light and leaf slopes. However, the application of LeafSpec was still limited by its low throughput and intensive labor cost in the field measurements. The goal of this project was to develop a robotic system that could replace the human operator to perform in-field and leaf-level HSI using LeafSpec. The system consisted of a machine-operable version of the LeafSpec device, a machine vision system for target leaf detection, and a customized cartesian robotic manipulator with five Degrees of Freedom (DOF). In the 2019 field test, the designed system collected data from corn plants with two genotypes and three levels of nitrogen treatments with an average cycle time of 86 s. The nitrogen content predicted by the designed system had an R<sup>2</sup> value of 0.7307 against the ground truth. The prediction could also differentiate the different nitrogen treatments with P-values of 0.0193 and 0.0102. The performance was similar to human operators'. The developers, therefore, conclude that the robotic system has the potential of replacing human operators for LeafSpec hyperspectral corn leaf imaging in the field.

## 1. Introduction

The world population is expected to grow by over a third, or 2.3 billion people by the end of 2050 (Eise and Foster, 2018). The challenge is to increase food production and do so in a sustainable way (Beddington, 2010). By connecting the genotype to the phenotype, high-yielding, stress-tolerant plants can be selected far more rapidly and efficiently (Li et al., 2014). Hyperspectral Imaging (HSI) technology has been explored and applied in plant phenotyping as both spatial and spectral information are obtained in a high-throughput and non-invasive way (Gowen et al., 2007). It can also detect the early onset of stresses and diseases, which would be beneficial to farmers and growers as it

would enable earlier interventions to help mitigate against crop loss and reduced crop quality (Lowe et al., 2017). As the stress and diseases can be detected earlier and more precisely, resources can also be saved.

There are many solutions for in-field HSI applications, but the data quality is affected by various noise factors. Currently, the typical use of HSI technology in agriculture is combining a Hyperspectral Camera (HSC) with an Unmanned Aerial Vehicle (UAV) or satellite to collect the top-view images of plants in the field, with high-throughput, under ambient light (Goetz, 2009). For higher resolution, a ground vehicle can be used in HSI to collect side-view images of the plants, under ambient light, in closer proximity (Goetz, 2009). Although these systems provide effective and high-throughput solutions for in-field phenotyping, their

<sup>\*</sup> Corresponding author at: Department of Agricultural and Biological Engineering, Purdue University, 915 W State St, West Lafayette, IN 47907, United States. E-mail address: jinjian@purdue.edu (J. Jin).

signal quality is compromised by various noise factors such as daylight variation, weather condition and surface angles of the plant leaves (Wang et al., 2020). Alternatively, there are also handheld devices equipped with an enclosed imaging chamber and independent lighting source to collect HS images at leaf-level to eliminate the in-field noise factors stated above. The most common design uses HSC to collect HS images of spots on the leaf, known as spectroradiometer (Ge et al., 2019). However, due to the significant variance of spectrum across the leaf (Yuan et al., 2016), taking the entire leaf image with a handheld touch-based HSC can provide higher measurement quality. The newest whole leaf HSI scanner, LeafSpec (Fig. 1), invented at Purdue University in 2018, has achieved such capability (Wang et al., 2020).

Although LeafSpec has the capability of taking HS images with high data quality, the collection of data is low-throughput and laborious. For each image collection, an operator needs to find the top-collared leaf of the target plant and then use LeafSpec to grasp gently and scan the leaf from the stem to the tip (Wang et al., 2020). This process requires the operator to stay focused throughout the measurements. The repeated scanning action can cause ergonomic stresses to the arm as well. Besides, the leaf scanning environment is typically bushy, moist, and often under hot summer weather conditions. Such long-time in-field manual HSI is a labor-intensive, slow and error-prone process (Vijayarangan et al., 2018). It would be ideal to improve the process of operating LeafSpec by replacing the human operator with a robotic system.

Various robotic arm systems have shown the capability of replacing human operators in using handheld HSI devices. The 3D perceptionbased collision-free robotic leaf probing technology was developed for automated indoor plant phenotyping (Bao et al., 2018). By combining a Time of Flight (TOF) camera with an articulated robotic arm, a portable spectrometer was shown to be capable of collecting leaf-level HS data in a greenhouse (Atefi et al., 2019). The author reported a grasping success rate of 78% for maize and 48% for sorghum. These systems are capable of automated probing or spectrometer measuring at one point, but not imaging an entire leaf. For in-field applications, a gantry robot has been used for HSI on plant-level to provide high-throughput data collection (Palli et al., 2019). In this imaging setup, there was open space between the camera and the plants, causing the HS data quality to be still affected by leaf surface slope and ambient light variations. The existing robotic solutions for leaf-level data collection were only capable of collecting point data in an indoor environment. A robotic system that could perform leaf-level HS data collection of an entire leaf in the field was in need.

The goal of this work was to design and implement a robotic system, by integrating existing technologies, to test the feasibility of using the robotic system to replace the human operator in leaf-level HS data collection with LeafSpec in a cornfield. The human operator of LeafSpec scans a leaf in three steps: 1) Identifying the top matured/collared leaf on the target plant; 2) Moving LeafSpec to the target leaf while avoiding

the other leaves around it;3) Grasping the leaf with the device to collect the HS data. Correspondingly, the five objectives of this work were:

- To design a machine vision system that can detect and obtain 3D coordinates of corn leaves.
- To design a robotic manipulator that can operate LeafSpec to collect HS data.
- To modify LeafSpec to improve its compatibility with the designed robotic system.
- 4. To investigate the path planning in the data collection process.
- To compare the data collected by the designed system with the ground truth data and historical data collected by human operators.

#### 2. Materials and methods

#### 2.1. Overview

In this robotic system, the leaf detection function was implemented with a vision system consisting of an Intel® RealSense<sup>TM</sup> Camera (Intel Corporation, U.S.), an NVIDIA® Jetson<sup>TM</sup> TX2 computer (NVIDIA Corporation, U.S.) and a pre-trained object detection algorithm deployed on TX2. A customized Cartesian manipulator and a control program, with path planning and velocity control, were used to grasp detected leaves. The scanning process was completed using a modified version of Leaf-Spec, which had a more compact size and lighter weight. The system was designed to be compatible with various mobile platforms. The finalized system mounted at the back of a research-use tractor, PhenoRover, is shown in Fig. 2.

For each scanning, the mobile platform stopped at the target plant. The vision system took a 3D image, recognized the target leaf, and

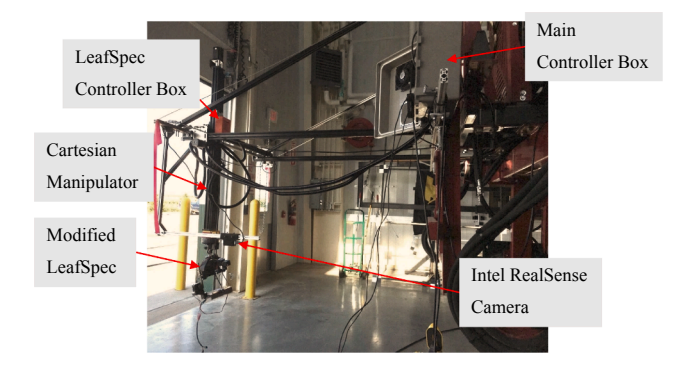


**Fig. 2.** An overview of the main components in the cartesian robotic platform mounted at the back of a semi-automated ground-based research vehicle: PhenoRoyer.

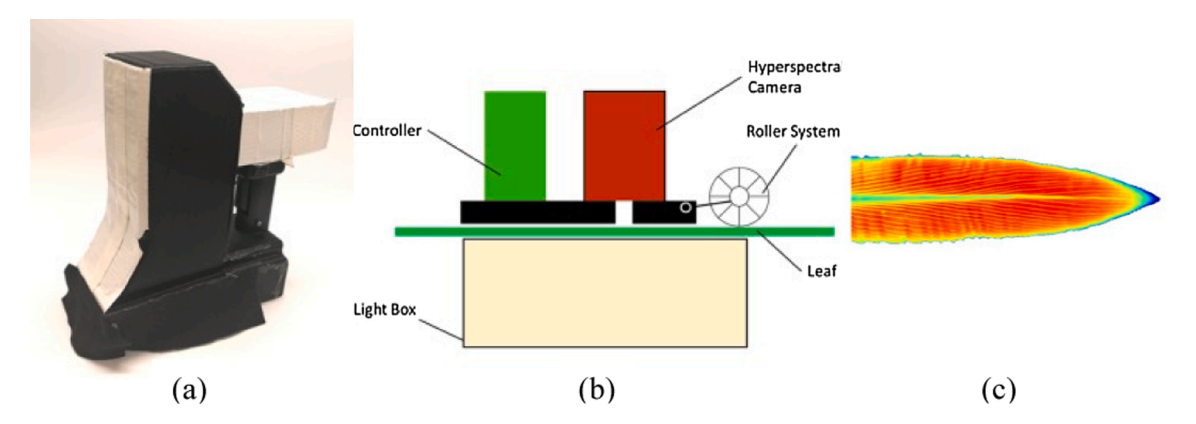


Fig. 1. An overview of LeafSpec (a), system schematic (b) and collected high-resolution Normalized Difference Vegetation Index (NDVI) heatmap (c) (Wang et al., 2020).

obtained its 3D coordinates. The control system, deployed on National Instruments<sup>™</sup> myRIO, generated a path and corresponding velocity profile for each motor on the manipulator. Finally, the manipulator followed the path to approach the leaf, grasped the leaf with the modified LeafSpec device and finished the scanning process. The videos of the operation stated above are available online (for the indoor test: https://www.youtube.com/watch?v=1bGeoLFSbjE, for the in-field test: https://www.youtube.com/watch?v=ZhNJeNjbsCY).

#### 2.2. Vision system

To detect and acquire the coordinates of the target leaf, an Intel® RealSense<sup>TM</sup> D435 camera was used to collect positional information. The Intel® RealSense<sup>TM</sup> depth camera D435 uses stereo matching to offer quality depth information.

Two rounds of image collection were conducted in a greenhouse for training the machine vision model. Each round had around 90 corn plants of two genotypes (B73xMo17 and P1105AM). Two nitrogen treatments (low and high) and two water treatments (low and high) were applied. There were 1138 images collected around the V7 stage using the Intel® RealSense™ D435 depth camera (approximately 70 to 100 cm from the target corn plant). The data set was then split into a training set and validation set with the ratio of 4:1 (910 and 228 images for each). The shape of each image data matrix was (720, 1280, 4), indicating its spatial resolution by pixel and four channels (R, G, B, Depth).

An open-source software, LabelMe (https://github.com/wkentar o/labelme), was used to manually annotate the images to get the ground truth (the location and growing direction) of every top-collared leaf within each image (Fig. 3).

A light, fast and accurate Convolutional Neural Network (CNN) architecture, Single Shot Multibox Detector (SSD) created at Cornell University (Liu et al., 2016), was used for the detection task. The original SSD architecture was modified using a different backbone network, the SE-ResNet50, which was pre-trained on opensource datasets iNaturalist 2017 and 2018.

During training, the original images were padded to maintain the aspect ratio and then resized to  $500 \times 500$ . During inferencing, the model would generate the most confident bounding box (Fig. 4) and its direction (left or right side of the stem). The result allowed the extraction of the sub-image and its matched depth array. The distance from the detected collar to the robotic arm could then be calculated by the corresponding depth array.

The mAP (mean Average Precision, a popular metric in measuring the accuracy of object detectors) on the training set reached 0.706, while the mAP on the validation set was 0.653. An entire prediction procedure (including preprocessing, inferencing and postprocessing) took approximately 0.2 to 0.3 s per image. The process was completed using the mxnet (v1.5.0) deep learning framework on an NVIDIA® Jetson TX2.

#### 2.3. Device modification

Since the original LeafSpec was designed to be operated by hand, adjustments were implemented to be compatible with the robotic system (Fig. 5). The manual grasping mechanism was replaced with a stepper motor, a set of rack and pinion, and a linear guideway. The HSC was added a 90-degree bend from vertical to horizontal to decrease the overall height. The weight of the device was reduced from 2.5 kg to 2 kg. The height was reduced from 150 mm to 95 mm, and the length and width remained the same. A signal wire was connected to the trigger pin on the LeafSpec controller from the manipulator controller, myRIO.

Since corn leaves do not have noticeable variance around the roll axis (Fig. 6), no Degrees of Freedom (DOF) was implemented for the roll angle. Corn leaves have variance in the pitch angle across their growing period and have the most variance in the yaw angle even at the same stage. Therefore, a turntable and a ball joint lock were installed between the manipulator and the modified device to provide additional DOFs. The modified LeafSpec device could be rotated around the yaw axis. The pitch angle of the device was adjusted manually and periodically to compensate for the angle change through each growing stage of corn plants.

### 2.4. Cartesian manipulator system

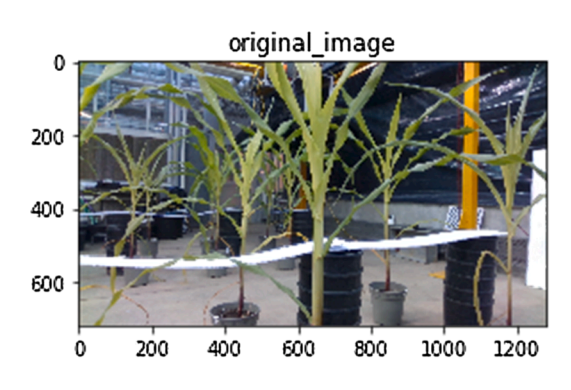
#### 2.4.1. Manipulator design

For robotic manipulators, Selective Compliant Assembly (SCARA), cylindrical, polar, jointed (articulated), and Cartesian are commonly used configurations. Each design has a unique workspace profile. The choice of manipulator type was determined based on the workspace requirement, in-field power efficiency, weight and flexibility for scanning motion.

Since the data collection using LeafSpec requires continuous scanning from the start of the leaf to the tip, to scan long leaves or reach further leaves in a cornfield, a manipulator needs a longer link length. However, for a manipulator with rotary joints, the increase in link length



Fig. 3. An example of labeled images used for training detection model with right growing direction (green boxes) and left growing direction (red boxes). (For interpretation of the references to colour in this figure legend, the reader is referred to the web version of this article.)



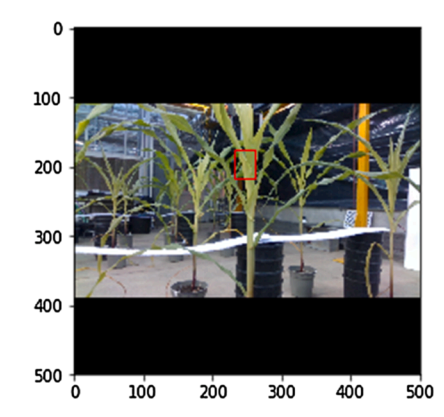


Fig. 4. The original image (left) and the predicted most confident bounding box (right) using the SSD detection algorithm developed by Cornell University.

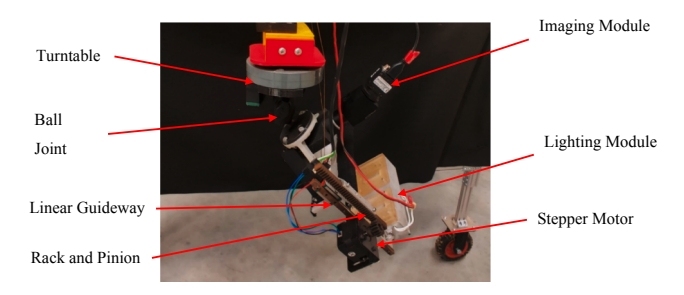
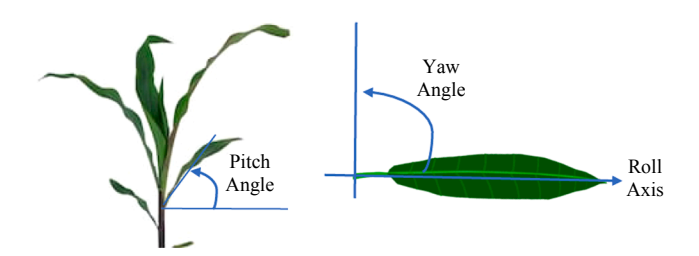


Fig. 5. An overview of the components of the modified LeafSpec mounted on the robotic arm.



**Fig. 6.** Side-view of the pitch angle (left) and top-view of the yaw angle (right) of corn leaves.

requires the manipulator to increase its power output exponentially (Lee and Lee, 1984). Consequently, the increase in power output increases overall weight, assuming a constant power-to-weight ratio. In contrast, a Cartesian manipulator only uses linear joints, so the change in link length does not require a change in motor power. As a result, the Cartesian configuration has a much smaller mass than non-Cartesian configurations under the same payload requirement. For the same reason, the cost of non-Cartesian manipulators, under the same dimension, power, and precision requirements, is generally higher than the cost of Cartesian manipulators.

Non-Cartesian manipulators also have less flexibility during configuration modification. Non-Cartesian manipulators generally have predetermined hardware configurations with corresponding sets of Equations of Motion (EOM). Therefore, hardware configuration changes require calculating a new set of EOM and checking for unsolvable poses. In comparison, the EOM of the Cartesian manipulator has a much simpler structure. Therefore, under the same power, weight, price, and flexibility constraints, the Cartesian configuration has a better performance compared to non-Cartesian designs for in-field leaf-level HSI of

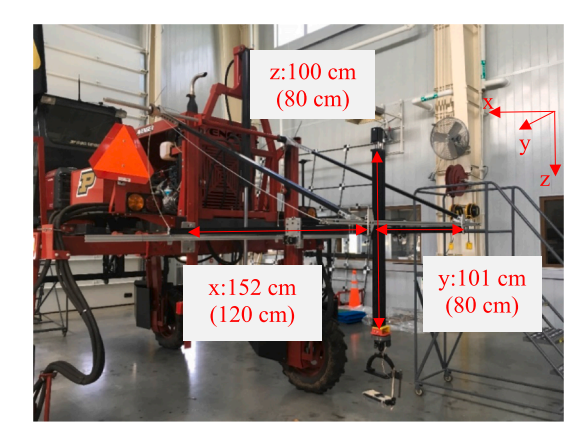


**Fig. 7.** Dimension and travel range (in parenthesis) of each axis of the designed robotic system. (The image was taken at the early stage of the development with circuits uninstalled at the time.)

corn plants.

The customized Cartesian robot was designed and constructed based on an existing motion system ACRO (Fig. 7) from OpenBuilds Part Store. ACRO is a positioning system with two DOFs (X and Y) with dimensions of  $60 \times 40$  in. (152  $\times$  101 cm). The ACRO system has two stepper motors along the x-direction and one stepper motor along the y-direction. Both directions are driven by toothed pulleys and timing belts. The maximum travel for the x-direction is 120 cm and 80 cm for the y-direction.

The third DOF (Z-axis) of the Cartesian robot was added by attaching a linear actuator to the mounting plate of the ACRO with a custom adapter. The installed linear actuator (C-Beam® Double Wide Gantry Actuator Bundle from OpenBuilds Part Store) (Fig. 7) uses a lead screw driven by a stepper motor to provide linear motion with a dimension of 100 cm and maximum travel of 80 cm.

# 2.4.2. Manipulator control

The manipulator's control algorithm was deployed on myRIO. The control program was developed using LabVIEW $^{\text{TM}}$  from National Instruments $^{\text{TM}}$ . The program included validations of the leaf detection results, path planning, velocity control of the manipulator, the open/close of the lightbox of the modified LeafSpec, and the start/end of the scanning process.

At the beginning of each scanning cycle, the leaf detection algorithm deployed on TX2 sent a set of coordinates to myRIO. A coordinate transformation was performed to transform the coordinate set from the RealSense's coordinate frame ( $x_c$ ,  $y_c$ ,  $z_c$ ) to the manipulator's coordinate

frame  $(x_r,\,y_r,\,z_r)$  using the following transformation matrix (Eq. (1)), where (dx, dy, dz) are the displacements between two coordinate systems. The (dx, dy, dz) were obtained by measuring the displacement from the origin of the robotic manipulator's coordinate frame to the origin of the RealSense camera's coordinate frame along the manipulator's coordinate frame axes.

$$\begin{bmatrix} x_r \\ y_r \\ z_r \\ 1 \end{bmatrix} = \begin{bmatrix} 1 & 0 & 0 & dx \\ 0 & 0 & 1 & dy \\ 0 & 1 & 0 & dz \\ 0 & 0 & 0 & 1 \end{bmatrix} \begin{bmatrix} x_c \\ y_c \\ z_c \\ 1 \end{bmatrix}$$
 (1)

where  $(x_c, y_c, z_c)$  are the coordinates in the camera frame and  $(x_r, y_r, z_r)$  are the coordinates in the manipulator frame.

After the coordinates were transformed, the set of coordinates was evaluated to determine if it was a valid set. The validations included determining: (1) if the coordinate set was empty; (2) if the scanning path, based on the given coordinates, surpassed the boundary of the workspace. If the validations failed, the control program would request a new set of coordinates.

To have independent control on each motor simultaneously, the field-programmable gate array (FPGA) in myRIO was used for controlling the five stepper motors (four on the manipulator, one on the device). The acceleration and deceleration were accomplished by using a trapezoidal velocity profile. In FPGA, such velocity control was implemented by changing the frequency of the signal generator in each thread according to a calculated velocity profile. The implemented control used open-loop control, assuming there was no skipped step. The upper limit of acceleration and deceleration of the manipulator were determined by testing the highest value when there was no step skipped. The step counter was calibrated after every scan iteration when the manipulator was rehomed, so the impact of skipped steps was minimal.

# 2.4.3. Path planning

LeafSpec requires a leaf to be in between its lightbox and camera. Without path planning, when the system moved the device toward the target location directly from its home position, LeafSpec would collide

with the target leaf because of the natural curvature of the leaf (Fig. 8). An insertion angle perpendicular to the target leaf on the x-y plane was maintained to avoid such collision.

The end position of the approaching process should not be close to the target plant's stem to provide clearance for the device. If the end position was too close, the device would hit the stem at the red region, as shown in Fig. 9. As a result, the whole plant would be pushed away, and the leaf would not be successfully grasped for scanning. Therefore, the end position was set to be away from the stem, but this would cause the loss of the scanned area. To solve this problem, when LeafSpec grasped the leaf, the device slid back towards the stem first to allow more area of the leaf to be scanned.

As shown in Fig. 10, the planned path would approach the target plant along the row direction and then approach the target leaf while



**Fig. 9.** Side-view of an example of the modified LeafSpec hitting stem with hitting region marked (red marked). (For interpretation of the references to colour in this figure legend, the reader is referred to the web version of this article.)

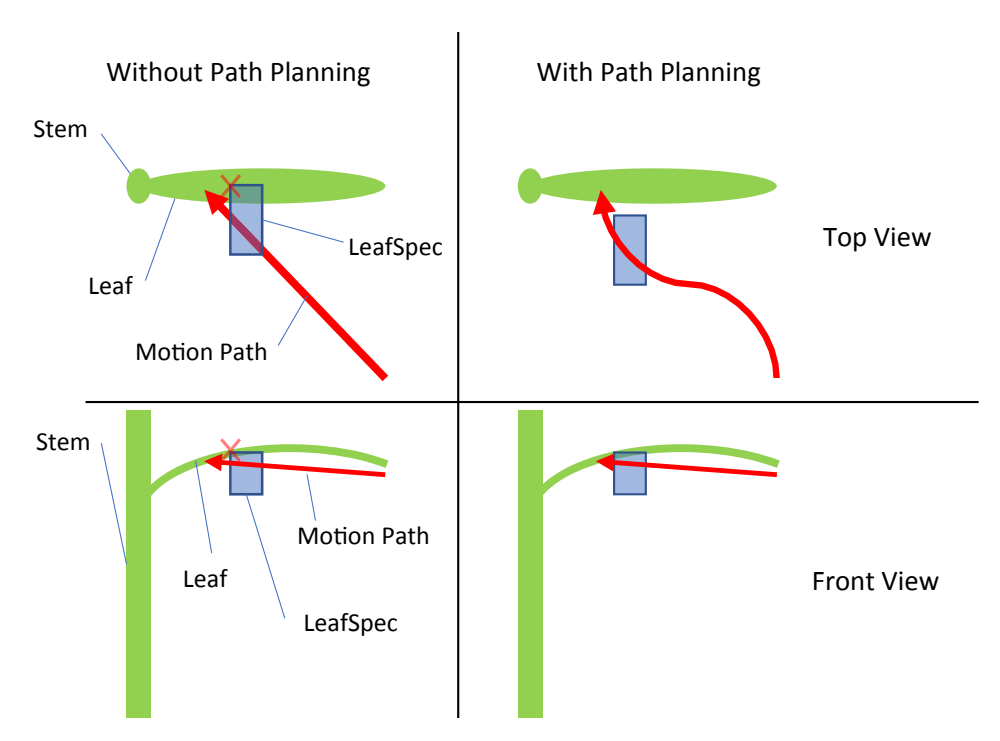
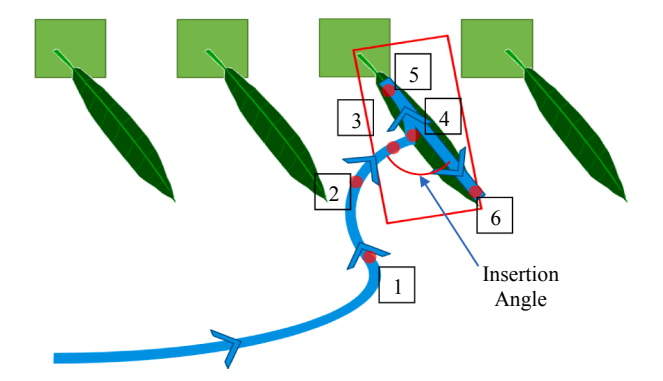


Fig. 8. Comparison of motion path with and without path planning in the top and front view: The possible collision happens at the red cross between LeafSpec and the lower surface of the target leaf when a 90 degrees insertion angle is not implemented. (For interpretation of the references to colour in this figure legend, the reader is referred to the web version of this article.)



**Fig. 10.** An example of a planned path for approaching the target plant/leaf (boxed) using generated waypoints to avoid collision with adjacent plants and the stem of the target plant. The blue path shows the desired path for the entire scanning process, and the red points indicate the waypoints generated from the path planning algorithm. (For interpretation of the references to colour in this figure legend, the reader is referred to the web version of this article.)

keeping the insertion angle around 90 degrees. Next, LeafSpec grasped onto the leaf at a location about 20 cm away from the stem. Then, it moved back to the stem to maximize scanning coverage. Finally, the controller triggered the scanning process.

The finalized path planning algorithm generated waypoints based on the procedures mentioned above. Four major waypoints were generated to control the approaching process, and two major waypoints were generated to control the scanning. The waypoints one to three represented the approaching path to the target plant. The 90-degree insertion angle was determined by waypoints three and four. Waypoint five drove the path towards the stem for a short distance to compensate for the coverage lost in Fig. 9. The last waypoint, waypoint six, represented the end of the scanning path. The expected cycle time of execution of all waypoints by the Cartesian robotic platform was about 45–50 s.

The waypoint generation was not in the same order as the execution. The following discussion follows the order of waypoint generation. Waypoint four was generated first, which was based on the detection results from the vision system. Since the detection results only returned the collar location of the target leaf, waypoint four  $(P_4)$  was calculated based on Eq. (2).

$$P_{4} = P_{collar} + l_{insert} \begin{bmatrix} \cos(\theta_{pitch})\cos(\theta_{yaw}) \\ \cos(\theta_{pitch})\sin(\theta_{yaw}) \\ -\sin(\theta_{pitch}) \end{bmatrix}$$
(2)

where

 $P_{collar}$  is the coordinate set returned by the vision system  $l_{insert}$  is the length between the stem and the insertion point along the leaf

 $\theta_{yaw}$  is the yaw angle of the target leaf  $\theta_{pitch}$  is the pitch angle of the target leaf

Waypoint three was calculated by Eq. (3).

$$P_{3} = P_{4} - l_{offset} \begin{bmatrix} sin(\theta_{yaw}) \\ cos(\theta_{yaw}) \\ 0 \end{bmatrix}$$
 (3)

where

 $l_{\it offset}$  is the distance between waypoint four and three (10 cm used here)

Waypoint five  $(P_5)$  was generated by Eq. (4). The variable K in the equation is an arbitrary number that determines how close the waypoint

five is to the stem. The higher the value, the closer the waypoint to the stem.

$$P_{5} = P_{4} - Kl_{insert} \begin{bmatrix} \cos(\theta_{pitch})cos(\theta_{yaw}) \\ \cos(\theta_{pitch})sin(\theta_{yaw}) \\ -\sin(\theta_{pitch}) \end{bmatrix}$$

$$(4)$$

where

K is an arbitrary number between 0 and 1

The waypoints one and two were generated so that the settling time in the x-direction from the home position to waypoint three was half of the settling time in the y- and z-direction. The path after such adjustment would go around the adjacent plants first and then approach the target plant to avoid colliding with the adjacent plants.

The waypoint six ( $P_6$ ) was generated by Eq. (5). The leaf length is a manual input parameter based on the stage at which corn plants are.

$$P_{6} = P_{5} + l_{leaf} \begin{bmatrix} \cos(\theta_{pitch})\cos(\theta_{yaw}) \\ \cos(\theta_{pitch})\sin(\theta_{yaw}) \\ -\sin(\theta_{pitch}) \end{bmatrix}$$
 (5)

where

l<sub>leaf</sub> is the length of the target leaf from the stem to the tip

# 2.4.4. Data flow

The structure of the data flow of the overall system is shown in Fig. 11. The TX2 acquired both RGB and depth images from Intel® RealSense<sup>TM</sup> camera. The RGB image was passed through the detection algorithm to obtain the x and y coordinates (in the camera's frame) of the target leaf. The depth image was then matched with the detection result to obtain the z coordinate of the leaf. The XYZ coordinates were then sent to myRIO for validation through Transmission Control Protocol (TCP). If the coordinates were valid, myRIO then calculated the path and velocity profile. Otherwise, myRIO asked for another coordinate set. MyRIO outputted control signals to the motor driver to drive the motors on the manipulator and triggered the modified LeafSpec to start scanning. The scanned results were then sent to smartphones for preview through Bluetooth.

# 2.5. Experiment setup

In a typical corn breeding project, nitrogen use efficiency (NUE) and water use efficiency (WUE) are the most popular and important plant phenotyping features to be collected, and the plant growth difference is evaluated under different nitrogen and water stresses. The experiment for demonstrating the capability of the new robotic system was set up in such a breeding phenotyping project setup. The experiment was conducted on October 4th, 2019, in the Agronomy Center for Research and Education (ACRE) field of Purdue University. Two genotypes

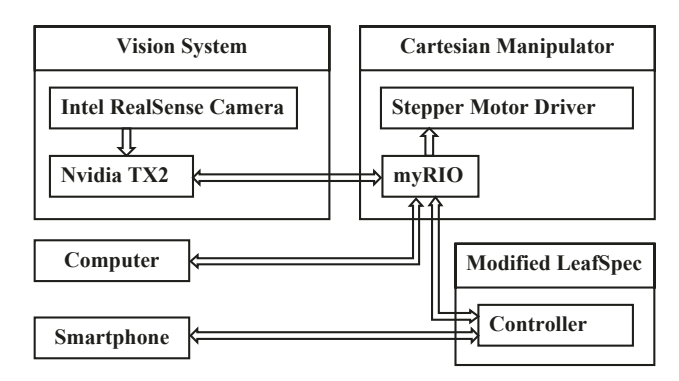


Fig. 11. Data flow of the designed system.

(B73xMo17 and P1105AM) were planted in 41 plots and treated with three nitrogen treatments (high, medium, low) to have the necessary nitrogen stress variance. Since water treatments could not be controlled in the field, no water treatments were applied. The experiment was performed when the plants reached the V8 stage (each plant had eight leaves with visible leaf collars). Since the research ground vehicle PhenoRover was under repair at the time, a customized ground-based mobile platform (Fig. 12) was built as an alternative. The platform was moved to the middle of each plot, and one nearby plant was randomly selected by the leaf detection algorithm deployed on TX2.

For each scanning, the detection algorithm returned an image labeled with a box indicating the detected top collar leaf. The manipulator was activated if the detection result was approved by the operator (automating the approval process is future work). If not, the system would restart the detection. The flowchart is shown in Fig. 13, where  $N_d$  is the number of detection needed before a correct top-collared leaf is detected and  $N_s$  is the number of scanning the manipulator performed before the target leaf is successfully scanned. A total of 41 plants were scanned by the designed system (Fig. 14). The HS raw data were saved on the local storage of the modified LeafSpec. After the scanning of each plant, the scanned leaf was cut and saved for nitrogen measurement by a commercial service company (A&L Great Lakes Laboratories, Inc). The measured nitrogen concentrations were used as the ground truth in this experiment.

#### 3. Results

#### 3.1. System performance

During the field experiment, the designed Cartesian robotic platform scanned 41 plants using the modified LeafSpec. For each scan trial, the following parameters were recorded: the number of leaf detections trails executed by the TX2 computer ( $N_d$ ), the number of actual scanning trials performed until a successful scan ( $N_s$ ) and the total cycle time ( $T_c$ ), from the execution of the first detection to the manipulator was rehomed.

The distributions of the number of detections and scans needed to collect HS data of one plant are shown in Fig. 15 and Fig. 16. The vision system could detect the target leaf and return valid coordinates within five trials for more than 68% of the time. A detection trial was successful when the top leaf collar of one plant in the field of view was completely enclosed by the bounding box with the highest confidence value. The failed attempts included detecting wrong objects (i.e., recognizing a folded leaf as a top collar) or detecting no collar. Such results could be the consequence of daylight changes, high variance in the background and shadows from the adjacent plants in the field. More in-field plant images will be helpful to train a more robust machine vision model for detecting target leaves in the future.

The designed system could perform the data collection using the

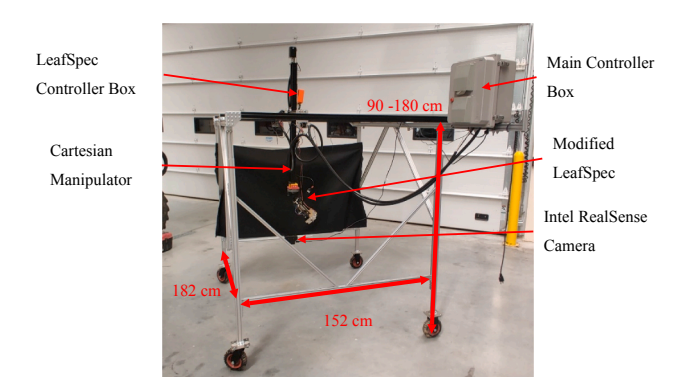
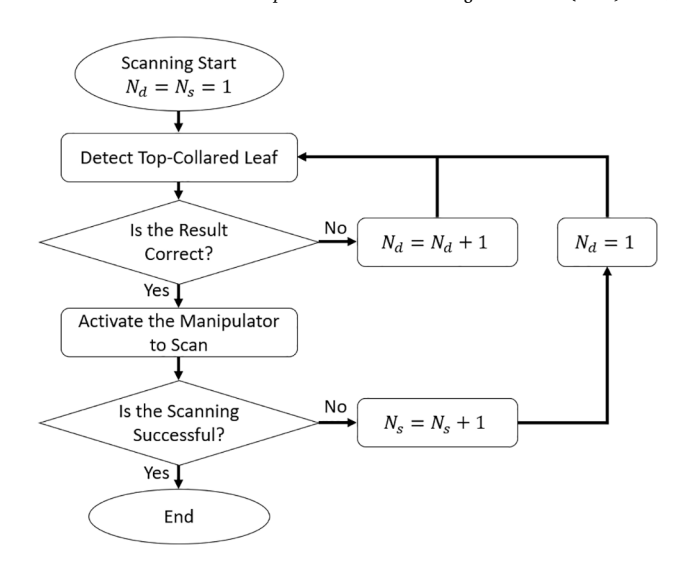


Fig. 12. An overview of an alternative mobile solution by mounting the designed robotic system on a customized wheeled platform with an adjustable height.



**Fig. 13.** Flowchart of data collection of each corn plant in the robotic system performance evaluation.

modified device successfully within two trials for 85% of the time based on correct leaf detection results. A scanning was successful when the image collected by the device contained a complete leaf without noticeable ambient light leaking into the imaging chamber. Such check was based on the spectrum quality it sent to the paired smartphone. In the manipulator's failed attempts, the vision system detected the top-collared leaf with a most confident bounding box, but the designed system failed to grasp the leaf by hitting or missing the leaves. One possible reason could be the movement of plant leaves due to the windy condition in the field. Since the collar detection and manipulator movement took time, the leaf's pose could be changed by the wind while the device was approaching the leaf. Another reason could be the error from image detection since the bounding box center was not guaranteed to locate at the leaf collar.

A total of 63 scanning trials were performed to finish scanning all the 41 plants. The cycle time, detection trials, scan trials, and damage conditions were recorded in Table 1. During the scanning of 41 plants, three leaves were damaged with different severities by the approaching and scanning process performed by the designed manipulator. One leaf had minor damage of broken leaf tissues. The other two leaves had relatively more severe damage of broken mid-rib. All leaves were damaged during failed scanning attempts. The average cycle time of the designed system was 86 s, with the distribution of all recorded cycle time shown in Fig. 17. The average cycle time of human operators scouting in the field was 64 s, which was calculated by dividing the total time of one round of data collection (from when the first plant was imaged to the last one) by the number of samples collected. The current velocity profile was limited by the torque delivered by the motors and could be improved in the future by adopting different motors. Although the designed system was slower than the human operator, the throughput could be improved by installing multiple copies of the robotic platform onto the vehicle to perform scanning at the same time. The variation of the cycle time mainly comes from the variation of  $N_d$  and  $N_s$  shown in Fig. 15 and Fig. 16. The relationship can be described by Eq. (6).

$$T_c = N_d T_d + N_s T_s \tag{6}$$

where

 $T_d$  is the time length of single execution of the detection  $T_s$  is the time length of single execution of the scanning

Although, on average,  $N_d > N_s$ , since  $T_d \ll T_s$  the cycle time is dominated by the number of scans performed.

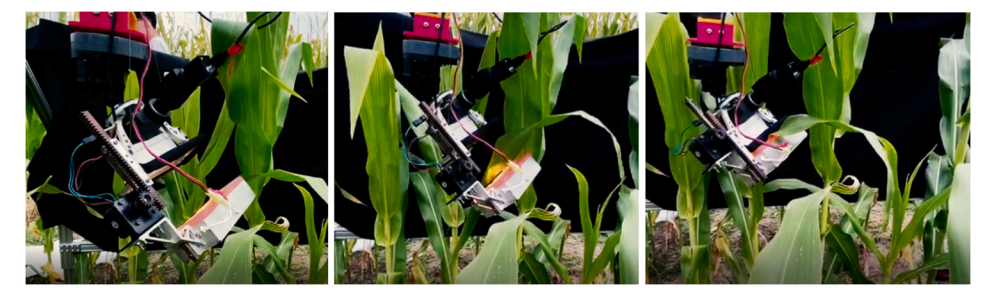


Fig. 14. Field demo of approaching (left), insertion (middle) and scanning (right).

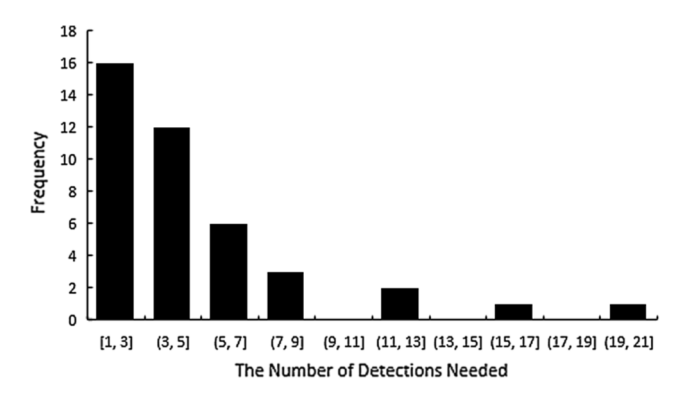


Fig. 15. Distribution of the number of detections needed for each plant.

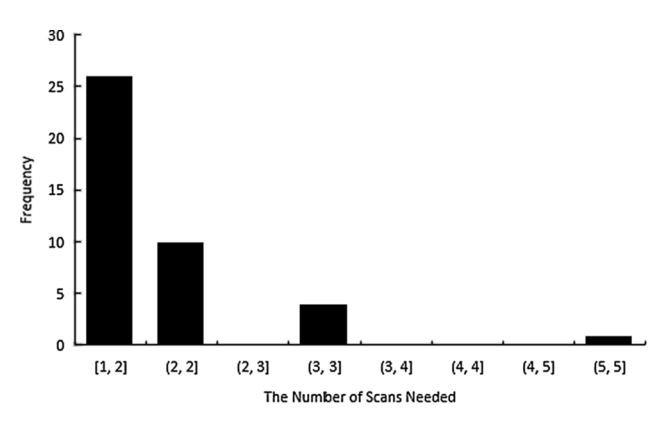


Fig. 16. Distribution of the number of scans needed for each plant.

**Table 1**In-field experiment results of the designed manipulator.

Parameters	Values
Total Plant Scanned	41
Average $N_d$	5.2
Average $N_s$	1.54
$\operatorname{Max} N_d$	21
$\operatorname{Max} N_s$	5
Total Damaged Plants	3
Fatal Damaged Plants	2
Average Cycle Time	86 s
Average Cycle Time by Human Operators	64 s

# 3.2. Scanning quality analysis

The collected HS raw data were processed using a nitrogen content prediction model. The model was built and used by the human-operated LeafSpec version (Wang et al., 2020). The model reads the HS raw data and outputs predicted nitrogen content. The nitrogen prediction model

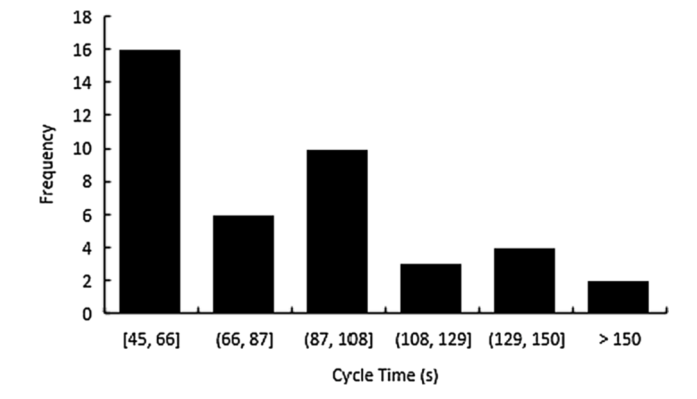


Fig. 17. Distribution of the recorded cycle time for all scanning.

was based on the averaged spectrum across all the pixels on the leaf. This "traditional" nitrogen prediction model was used in this study solely to compare the imaging quality between the human-operated version and the robotic version.

A box diagram was plotted for the relationship between the calculated nitrogen index and the nitrogen treatments (Fig. 18). T-tests were performed between different nitrogen treatments. The P-value between high and medium is 0.0193. The P-value between Medium and Low is 0.0102. The P-values indicate that the data collected by the designed system can provide enough statistical differences for differentiating different nitrogen treatments.

A scatter plot, which shows the relationship between the predicted and ground truth nitrogen content, was plotted (Fig. 19). This chart contains 38 data points because three sets were lost during the field test due to memory error. The plot shows that the nitrogen content predicted based on the data collected by the designed system has a high correlation with the ground truth data. Such correlation indicates the designed system can collect data with a quality able to reflect ground truth nitrogen content.

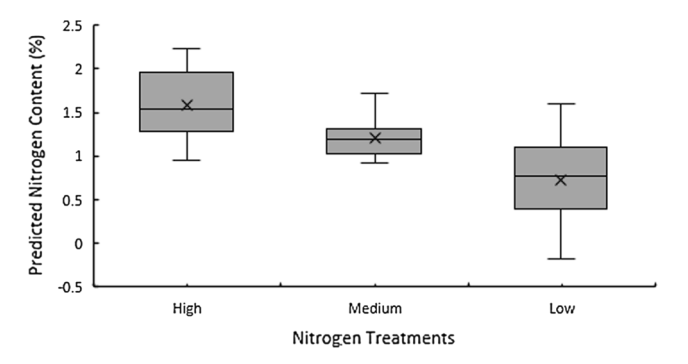


Fig. 18. Calculated nitrogen index vs. nitrogen treatments with a P-value of 0.0193 between high and medium and a P-value of 0.0102 between medium and low.

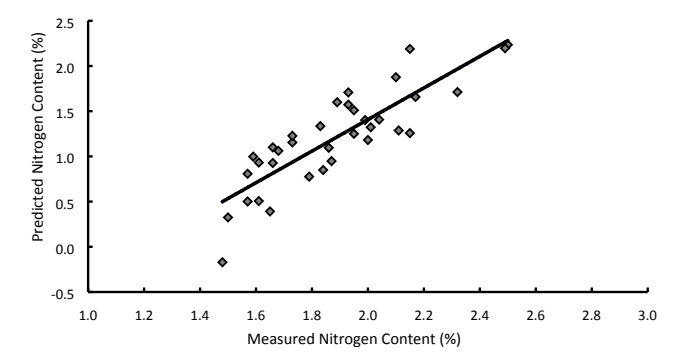


Fig. 19. Correlation between predicted nitrogen content (y) and measured nitrogen ground truth (x) with an  $\mathbb{R}^2$  of 0.7307.

Fig. 19 shows a strong correlation between the calculated nitrogen content and the measured nitrogen ground truth data. The  $\rm R^2$  value of the predicted nitrogen content with respect to ground truth measurement is 0.7307. This prediction performance was compared with the historical nitrogen content prediction performances by human-operated LeafSpec in 50 greenhouse and field assays during 2018–2019. The distribution of the historical nitrogen prediction  $\rm R^2$  by the human-operated LeafSpec is shown in Fig. 20. The  $\rm R^2$  value of 0.7307 by the robotic system lies in the middle of the 95% interval of the manual system's  $\rm R^2$  distribution. Therefore, it is concluded that the data collected by the robotic system can provide the HS data quality similar to the one collected by human operators.

## 4. Conclusion

In this paper, a Cartesian robotic platform was designed and developed to replace the human operator in collecting HS images of corn leaves in the field using LeafSpec, a proximal high-resolution hyperspectral leaf imager.

- An object detection machine vision model was trained to detect the top matured leaf as the target for scanning.
- A control program, including velocity control and path planning, was developed on LabVIEW™ and deployed on myRIO for the Cartesian manipulator.
- The system was successfully tested in a corn phenotyping project at Purdue's research farm in fall 2019 and collected images with accepted quality for all 41 plants, with 86 s cycle time on average.
- The plant nitrogen content prediction based on the HS images collected by the robotic system has an R<sup>2</sup> of 0.7307 with the ground truth measurements, which is comparable with the images collected by human operators in previous greenhouse and field assays. The prediction result also shows significant differences between nitrogen treatments.

Although the current averaged cycle time may not meet the throughput requirements in all phenotyping activities, there is great potential to improve the throughput with upgraded hardware and better control algorithms or multiple manipulators scanning leaves in parallel at the same time.

## CRediT authorship contribution statement

Ziling Chen: Conceptualization, Methodology, Software, Writing original draft, Investigation, Visualization, Data curation. Jialei Wang: Resources, Writing - review & editing. Tao Wang: Software. Zhihang Song: Software, Resources, Investigation. Yikai Li: Resources, Investigation. Yuanmeng Huang: Resources, Investigation. Liangju Wang: Validation. Jian Jin: Supervision, Project administration, Funding acquisition, Writing - review & editing.

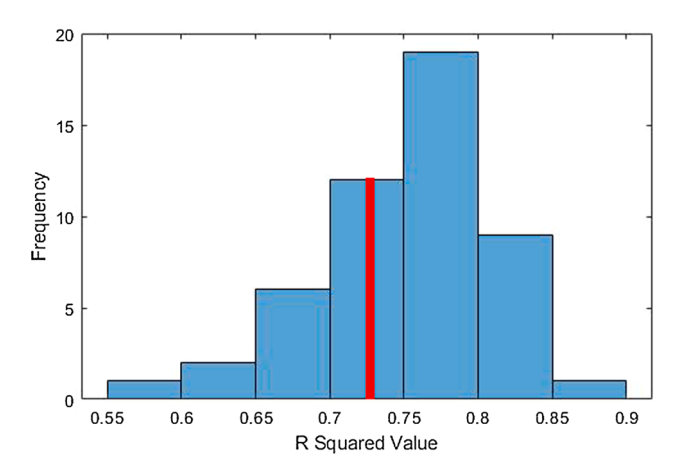


**Fig. 20.** Distribution of  $R^2$  of Historical LeafSpec Data with  $R^2$  of the Designed System (red line). (For interpretation of the references to colour in this figure legend, the reader is referred to the web version of this article.)

# **Declaration of Competing Interest**

The authors declare that they have no known competing financial interests or personal relationships that could have appeared to influence the work reported in this paper.

# Acknowledgments

This work was partially funded by TRASK TRUST Fund from Purdue Research Foundation. The authors would like to thank Jason A. Adams and Andrew G. Linvill from Indiana Corn and Soybean Innovation Center at Purdue University for providing support with field resources in this project, and Meng-Yang Lin from the Tuinstra Lab for his professional knowledge in ground truth data collection and validation.

#### References

Atefi, A., Ge, Y., Pitla, S., Schnable, J., 2019. In vivo human-like robotic phenotyping of leaf traits in maize and sorghum in greenhouse. Comput. Electron. Agric. 163 (June) https://doi.org/10.1016/j.compag.2019.104854.

Bao, Y., Shah, D., Tang, L., 2018. 3D Perception-based collision-free robotic leaf probing for automated indoor plant phenotyping. Trans. ASABE 61 (3), 859–872. https://doi. org/10.13031/trans.12653.

Beddington, J., 2010. Global food and farming futures. Philosoph. Trans. Roy Soc. B: Biolog. Sci. 365 (1554), 2767. https://doi.org/10.1098/rstb.2010.0181.

Eise, J., Foster, K., 2018. How to feed the world. How to Feed the World 1–250. https://doi.org/10.5822/978-1-61091-885-5.

Ge, Y., Atefi, A., Zhang, H., Miao, C., Ramamurthy, R.K., Sigmon, B., Yang, J., Schnable, J.C., 2019. High-throughput analysis of leaf physiological and chemical traits with VIS-NIR-SWIR spectroscopy: A case study with a maize diversity panel. Plant Methods 15 (1), 1–12. https://doi.org/10.1186/s13007-019-0450-8.

Goetz, A.F.H., 2009. Three decades of hyperspectral remote sensing of the Earth: A personal view. Remote Sens. Environ. 113 (SUPPL. 1), S5–S16. https://doi.org/ 10.1016/j.rse.2007.12.014.

Gowen, A.A., O'Donnell, C.P., Cullen, P.J., Downey, G., Frias, J.M., 2007. Hyperspectral imaging - an emerging process analytical tool for food quality and safety control. Trends Food Sci. Technol. 18 (12), 590–598. https://doi.org/10.1016/j. tifs.2007.06.001.

Lee, C.S.G., Lee, B.H., 1984. Resolved Motion Adaptive Control for Mechanical Manipulators. Proc. Am. Control Conf. 1 (June), 314–319.

Li, L., Zhang, Q., Huang, D., 2014. A review of imaging techniques for plant phenotyping.
 Sensors (Switzerland) 14 (11), 20078–20111. https://doi.org/10.3390/s141120078.
 Liu, W., Anguelov, D., Erhan, D., Szegedy, C., Reed, S., Fu, C.-Y., Berg, A.C., 2016. SSD: Single Shot MultiBox Detector. In: Leibe, B., Matas, J., Sebe, N., Welling, M. (Eds.), Computer Vision – ECCV 2016. Springer International Publishing, pp. 21–37.

Lowe, A., Harrison, N., French, A.P., 2017. Hyperspectral image analysis techniques for the detection and classification of the early onset of plant disease and stress. Plant Methods 13 (1), 80. https://doi.org/10.1186/s13007-017-0233-z.

Palli, P., Liew, C., Drozda, A., Mwunguzi, H., Pitla, S.K., Walia, H., Ge, Y., 2019. Robotic gantry for automated imaging, sensing, crop input application, and high-throughput analysis. In: 2019 ASABE Annual International Meeting, pp. 2–11. https://doi.org/ 10.13031/aim.201901519.

Vijayarangan, S., Sodhi, P., Kini, P., Bourne, J., Du, S., Sun, H., Poczos, B.,
Apostolopoulos, D., Wettergreen, D., 2018. High-Throughput Robotic Phenotyping

of Energy Sorghum Crops. In: Hutter, M., Siegwart, R. (Eds.), Field and Service Robotics. Springer International Publishing, pp. 99–113. Wang, L., Jin, J., Song, Z., Wang, J., Zhang, L., Rehman, T.U., Ma, D., Carpenter, N.R., Tuinstra, M.R., 2020. LeafSpec: An accurate and portable hyperspectral corn leaf

imager. Comput. Electron. Agric. 169 (January), 105209. https://doi.org/10.1016/j.

compag.2019.105209. Yuan, Z., Cao, Q., Zhang, K., Ata-Ul-Karim, S.T., Tan, Y., Zhu, Y., Cao, W., Liu, X., 2016. Optimal leaf positions for SPAD meter measurement in rice. Front. Plant Sci. 7 (MAY2016), 1–10. https://doi.org/10.3389/fpls.2016.00719.